ELSEVIER

Journal of Structural Geology 26 (2004) 1483–1498

JOURNAL OF STRUCTURAL GEOLOGY

www.elsevier.com/locate/jsg

Deformation mechanisms in second-phase affected microstructures and their energy balance

Marco Herwegh*, Alfons Berger

Institute of Geological Sciences, University of Bern, Baltzerstrasse 1, 3012 Bern, Switzerland

Received 17 December 2002; received in revised form 25 October 2003; accepted 31 October 2003

Available online 23 January 2004

Abstract

Based on the relationship Zener parameter (Z = second-phase size/second-phase volume fraction) vs. calcite grain size (d_g), second-phase controlled aggregates and microstructures that are weakly affected by second-phases are discriminated. The latter are characterized by large but constant grain sizes, high calcite grain boundary fractions and crystallographic preferred orientations (CPO), while calcite grain size and calcite grain boundary fraction decrease continuously and CPO weakens with decreasing Z in second-phase controlled microstructures. These observations suggest that second-phase controlled microstructures predominantly deform via granular flow because pinning of calcite grain boundaries reduces the efficiency of dynamic recrystallization favoring mass transfer processes and grain boundary sliding. In contrast, the balance of grain size reduction and growth by dynamic recrystallization maintains a steady state grain size in microstructures that are only weakly affected by second-phases promoting a predominance of dislocation creep. With increasing temperature, the relationship between Z and d_g persists but the calcite grain size increases continuously. Based on microstructures, the energy of each modifying process is calculated and its relative contribution is compared with energies of the competing processes (surface energy, dragging energy, dynamic recrystallization energy). The steady state microstructures result from a temperature-dependent energy minimization procedure of the system.

Keywords: Polyphase-rocks; Zener drag; Deformation mechanisms; Steady state; Microstructures; Energies; Calcite

1. Introduction

In natural environments, mylonitic microstructures are one important key to gain information about the mechanisms, conditions and kinematic framework of ancient deformation. Within high strain shear zones, steady state microfabrics develop whose microstructural parameters are adapted to the ambient physical–chemical conditions of deformation (Means, 1981; Knipe, 1989). In monomineralic materials, the mean grain size as prominent microstructural feature, for example, approaches a stable value, which is maintained by a balance of grain growth and grain size reducing mechanisms like nucleation or subgrain rotation recrystallization (Means, 1981; Lister and Snoke, 1984; Derby and Ashby, 1987; Herwegh et al., 1997; de Bresser et al., 1998; Shimizu, 1998). In such systems the grain size depends on differential stress (Mercier et al., 1977; Twiss, 1977; Poirier, 1985), type of recrystallization mechanism (Schmid et al., 1980; Tungatt and Humphreys, 1981; Rutter, 1995), nucleation type (Derby and Ashby, 1987; Shimizu, 1998) and temperature (de Bresser et al., 1998). In terms of deformation mechanisms, grain size, shape preferred orientation (SPO) and/or crystallographic preferred orientation (CPO) are used to draw inferences about the dominant deformation mechanism (e.g. Pauli et al., 1996; Bestmann et al., 2000; Mauler et al., 2001). For viscous flow, these mechanisms can be subdivided into two major groups: (1) dislocation creep and related mechanisms, and (2) granular flow including different diffusion controlled deformation mechanisms (e.g. see de Bresser et al., 2002). It was realized, however, that viscous deformation in rocks generally occurs by the simultaneous activity of different deformation mechanisms but the contribution of the individual mechanisms may vary as a function of the physical conditions (Walker et al., 1990).

In nature, monomineralic rocks are very rare and polyphase rocks cover almost entirely the earth's lithosphere. Experiments and theoretical studies show that bulk strengths can be (a) higher (Walker et al., 1990; Dresen

* Corresponding author. Tel.: +41-31-631-8764; fax: +41-31-631-4843.
E-mail address: marco.herwegh@geo.unibe.ch (M. Herwegh).

0191-8141/$ - see front matter © 2004 Elsevier Ltd. All rights reserved.
doi:10.1016/j.jsg.2003.10.006

et al., 1998), (b) situated between (Tullis et al., 1991; Handy, 1992; Ji et al., 2001) or (c) even below (Olgaard, 1990; Bruhn et al., 1999) the strengths of an individual mineral component incorporated in the polymineralic system. Hence, the extrapolation of experimental and theoretical implications to natural conditions is problematic for polyphase mylonites. For example, volume proportion, grain size, CPO and SPO of each individual mineral are variable parameters, which all can influence both microstructure and bulk rheology (e.g. Kruse and Stünitz, 1999). At the moment, our knowledge is too limited to really understand how these parameters are related to changes in stress, temperature and strain rate in polymineralic materials. With regard to grain size, for example, it is unclear how the different minerals influence each other and what the relation to variable contents of the different phases is. Does a steady state grain size also exist for polymineralic mylonites? Moreover, the occurrence of mineral interfaces can induce shifts in type of intergranular deformation and recovery behavior of the matrix minerals resulting in significant departure from the deformational behavior of the pure end member substance. Though granular flow and dislocation creep also predominate deformation of polymineralic systems their individual contribution to deformation of the bulk aggregate remains unclear.

In this study, we quantitatively investigate the influence of second-phases on calcite-dominated mylonites. The first part describes the microstructural changes in steady state microfabrics as a function of variable second-phase content, grain size and temperature. Based on this data set we present in a second step a new concept, which is based on an energy balance between retardation and driving forces for grain boundary migration at variable amounts of second-phase minerals. In contrast to classical nonhydrostatic thermodynamic approaches, the concept is directly linked to the quantified microstructural parameters and might therefore present a useful tool for the general description and interpretation of impure mylonites.

2. Analytical methods

The polyphase carbonate mylonites investigated were cut into rock prisms of x, y and z dimensions of about $4.5 \times 2 \times 1$ cm. The x–y plane is defined by the foliation, the prism's x-axis is parallel to the lineation and z is perpendicular to the foliation. In order to analyze the microstructure, the prisms were polished and treated afterwards by two-step etching (see Herwegh, 2000; Herwegh and Jenni, 2001). SEM imaging and image analysis software (NIH Image 1.62) were used to quantify grain sizes (equivalent circular diameter), aspect ratios of grains (minor divided by major grain axis), volume proportions, length of calcite grain boundaries and interfaces for both the calcite and second-phase minerals. Although working on digital images, time-consuming manual adjustments were required to allow an accurate segmentation of calcite and second-phase grains for the calculation of the aforementioned microstructural features. In the context of this paper, the total sum of the lengths of both calcite grain boundaries and interfaces are treated as the boundary total while the individual proportions are referred to as the calcite grain boundary and interface fractions. In terms of the microstructure quantification we did not attempt to extrapolate our data set towards the 3-D space for two reasons: (a) 3-D extrapolation usually is based on simplified assumptions about particle shapes. In the case of our polymineralic samples with highly variable mineral content and grain shape anisotropies such an extrapolation would involve a high degree of uncertainty. (b) It is known that due to sectioning effects in 2-D, i.e. apparently too many small grain sizes, a 2-D grain size distribution might deviate from a real 3-D one (e.g. Heilbronner and Bruhn, 1999). We reduced this problem for matrix grains, however, by using area weighted grain size distributions, where instead of weighting the size classes per number of grains, the area fraction per size class is calculated. In this way, the influence of larger grains is taken into consideration because they occupy more volume than small ones. With this step, the grain sizes shift close to approximated 3-D ones.

Crystallographic textures were analyzed by taking digital images from ultrathin sections using the program geovision (GV) and an automatic rotation polarization stage (Fueten, 1997; Fueten and Goodchild, 2001). GV was applied to automatically detect the grain boundaries and calculate c-axis orientations on grid nodes within a grid of 15×15 pixels (Goodchild and Fueten, 1998). While the accuracy in the derived c-axis trend is good ($< 2°$), the initial quality of the plunge measurements is weak because low and high inclinations are only weakly resolved (Fueten and Goodchild, 2001). For that reason, a sample whose texture was pre-analyzed with EBSD was analyzed with the GV-system allowing then a correction of the plunge and therefore an improvement in the data quality. Nevertheless, errors in the range of $10-20°$ have to be assumed. The corrected c-axis data were plotted in a stereonet and then contoured with the computer program GEOrient 9.1 (Rod Holcombe). Note that GV cannot distinguish between a c-axis with the same plunge but opposite trends. In a second step, the grain sizes were analyzed in the automatically generated grain boundary map applying the calculation procedure as was done for etched rock prisms.

3. Geological setting and sample description

3.1. Regional scale

For this study, four samples were collected at different localities along the basal thrust of the Doldenhorn nappe (Herwegh and Jenni, 2001), a compartment of the Helvetic

nappe stack in Central Switzerland. The Doldenhorn nappe reflects a former sedimentary basin that has been inverted and transposed to a large-scale recumbent fold during northwestward thrusting in a late stage of the Alpine Orogeny (Burkhard, 1988). The total displacement is in the range of 8–15 km and has been accommodated in a shear zone with a width of 1–10 m. Combined calcite–dolomite and calcite–graphite thermometry show that the temperature increases from NW to SE yielding temperatures of 340, 350, 356 and 400 °C for the four samples investigated. Although an error of ±30 °C results for the absolute temperatures, calcite–graphite thermometry indicates that differences in relative temperatures are as good as ±5 °C between the individual locations.

3.2. Mesoscale

On the outcrop scale down to the size of a hand specimen, carbonate mylonites with a dark gray color predominate in the shear zone Additionally, calcite veins dissect these mylonites, i.e. pure calcite, of variable relative age and deformational overprint. With increasing deformation the veins first become boudinaged and smeared out parallel to the shear plane. At high strains, the former calcite veins form parallel layers with the gray mylonites (Fig. 1). In this way a cyclical behavior of vein formation and deformation manifests the presence of fluids during deformation (see also Herwegh and Kunze, 2002).

3.3. Microscale

In terms of microstructures (a) low to moderately strained vein calcites have to be distinguished from (b) strongly deformed vein calcite and dark gray mylonites

(a) Prior to deformation, grain size in vein calcites is rather large (several 100 μm to several millimeters). In addition, this rock type contains only a very limited amount of quartz and sheet silicates as second-phase minerals. With increasing shear strain, the vein calcite becomes intensively affected by twinning and dynamic recrystallization resulting in a drastic grain size reduction (see also fig. 3 in Herwegh and Kunze, 2002). While the grain size distribution is bimodal and the veins are boudinaged at low shear strains, the geometry of the former veins becomes more and more parallel to the shear plane with increasing shear strain.

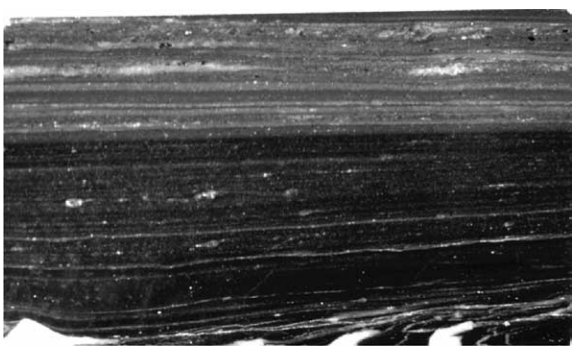

Fig. 1. Parallel layers of pure calcite (white) and calcite with different second-phase fractions (gray) in rock prism deformed at 400 °C. Horizontal dimensions 4.5 cm.

(b) High strain samples generally comprise several tens to a few 100-μm-thick layers, which are parallel to each other and the thrust plane. Boudinage is completely absent. Due to the lack of strain markers finite strains cannot be estimated. Based on the shear zone width and the known nappe displacement the samples must have seen very high shear strains. The second-phase content between the different layers varies from 0.5 vol% (high strain vein calcite) up to 12 vol% (Fig. 2). Sheet silicates are the major second-phase constituents, while only subordinate amounts of dolomite and quartz occur. Within each layer the second-phases are homogeneously distributed and occur as isolated individuals. Hence, the second-phases do not form an interconnected framework. Second-phases occur in grain interiors and on grain boundaries. In the case of impure samples they are preferentially situated along calcite grain boundaries while a more homogeneous distribution is found in purer samples (Fig. 2). The latter is especially the case for small sized equidimensional grains like dolomite but not for the sheet silicates with their high aspect ratios. The size of the second-phases range from a micron up to 100 μm and are therefore referred to as micron-scale second-phase particles. According to Herwegh and Kunze (2002), nano-scale second-phase particles like highly structured kerogens, dolomite and pyrite additionally occur. However, their influence on the average calcite grain size is much less dramatic than that of the micron-scale ones. For that reason, nano-scale minerals are not treated in further detail in the context of this work. Besides variations in grain size between individual layers, both matrix grain size of pure layers and the size of the sheet silicates increases with increasing metamorphic conditions (see also Herwegh and Jenni, 2001).

4. Microfabric quantification

4.1. Zener parameter

Figs. 2 and 3 show that in the samples investigated the calcite grain sizes vary as a function of the size (d_p) and volume proportion (f_p) of second-phase minerals (for abbreviations see Table 1). Hence, the second-phase minerals affect the calcite grain size. The influence of second-phases on the migration of grain boundaries of a matrix mineral is called Zener drag because it was recognized first by Zener (cited in Smith, 1948; see also Stüwe, 1978; Nes et al., 1985; Evans et al., 2001). Based on Zener drag, a relationship between stable matrix grain size (d_g) and the size (d_p), volume fraction (f_p) and a geometric factor (m) of second-phases in the form of a power law

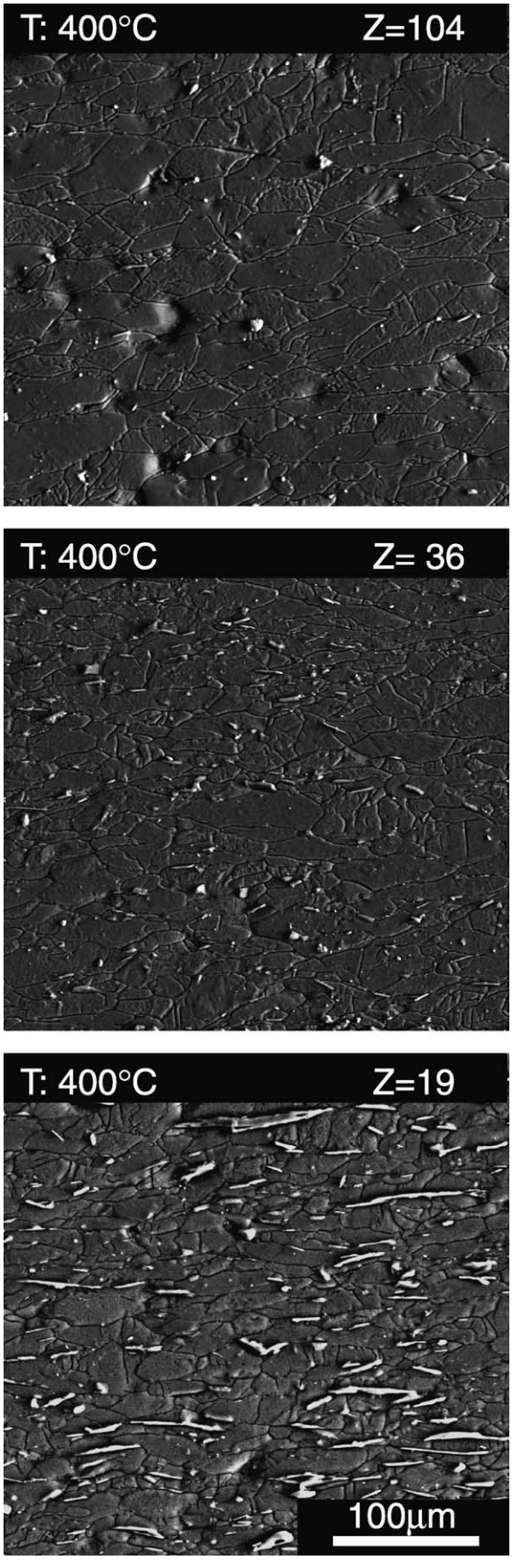

Fig. 2. Microstructural variations as a function of changes in second-phase content within a sample deformed at 400 °C. Electron backscatter image of polished rock surface after two-step etching. Second-phases = bright grays, micas = elongated grains, quartz and dolomite = small equiaxed grains.

exists (see Evans et al., 2001 and references therein):

$$d_g = Cd_p/f_p^m \quad (1)$$

where C is an empirically determined constant. Although established and applied for grain growth under static conditions, we modify Eq. (1) for our deformed polymineralic aggregates in the following manner:

$$d_g = CZ^{m*} \quad (2)$$

where $Z = d_p/f_p$.

In contrast to the original definition, we use $m*$ as power to Z, which we will refer to as the Zener parameter (Z) in the following. This parameter is a convenient measure because it is sensitive to both variations in grain size and volume fractions of the second-phase particles (Fig. 3). For example, large f_p and small d_p, respectively, at constant d_p and f_p both result in a small Zener parameter (Fig. 3, left column). In contrast, high parameters are obtained for microstructures with small f_p and large d_p at constant d_p and f_p, respectively (Fig. 3, right column). In nature, any transition between these four end members can be expected to occur.

4.2. The relationship between Zener parameter and microfabric

In order to study the influence of the second-phases onto the grain size of the matrix calcite, we tried to keep as many physical parameters as possible constant. (a) All sample areas investigated derive only from the high strain parts and therefore represent steady state microfabrics. (b) Whenever possible, microstructural analyses were performed in areas with a layer parallel geometry. (c) Only areas with homogeneous second-phase and size distribution were investigated. (d) Within a single sample prism with dimensions of only a couple of centimeters, temperature gradients are very unlikely to occur and therefore the temperatures are interpreted to be constant.

The data obtained for the following treatment are available in the form of an extensive table upon request from the authors.

4.3. Microstructural changes at constant T

The log–log diagram of Fig. 4 shows the grain size of the matrix calcite as a function of the Zener parameter for samples deformed at four different temperatures. Generally, the diagram can be separated into two parts. In the left part, with $Z < 100$, the calcite grain size increases for all samples with increasing Zener parameter. For Zener parameters

Table 1
Abbreviations used

Abbreviation	Explanation	Measured unit	Used unit
d_g	Grain size of matrix minerals	μm	μm
d_p	Grain size of second phase particles	μm	μm
f_p	Volume fraction of second phase particles		
s_g	Total grain boundary length of matrix minerals	μm	Calculated in m
n_p	Number of second phase particles		Dimensionless
T	Temperature		°C
x_p	Long axes of a grain	μm	Only used for ellipcity
y_p	Short axes of a grain	μm	Only used for ellipcity
E_p	Ellipticity of second phase particle (y_p/x_p)		Dimensionless
γ_A	Surface energy of the mineral A		J/m^2
L	Dragging length		m
L_p^{tot}	Sum of all dragging distances		m
D_{dis}	Dislocation density		m^{-2}
b	Burgers vector	Å	m
R	Outer radius of the volume around a dislocation	Å	m
r_0	Inner radius of the volume around a dislocation	5b	m
μ	Shear modulus		Pa
ν	Poisson ratio		Dimensionless
E	Energy of a screw or edge dislocation		J
G^{tot}	System's total free energy		J/m^2
G_{fabric}	Fabric free energy		J/m^2
G_{surf}	Surface free energy		J/m^2
G_{drag}	Total dragging energy		J/m^2
$G_{dyn.recr.}$	Dynamic recrystallization energy		J/m2
G_{dcr}	Strain energy related to dislocation creep		J/m^2
G_{grf}	Strain energy related to granular flow		J/m^2
F_{drag}^{p}	Dragging force per particle		N
F_{drag}^{tot}	Total dragging force per unit area		N
Z	Zener-parameter (d_p/f_p)		μm

$\geqslant 100$ the calcite grain sizes do not vary anymore with increasing Z and therefore represent characteristic values, which are constant at each temperature. For this reason, we will refer to microstructures with Z smaller and larger than 100, respectively, as second-phase controlled microstructures and microstructures weakly affected by second-phases.

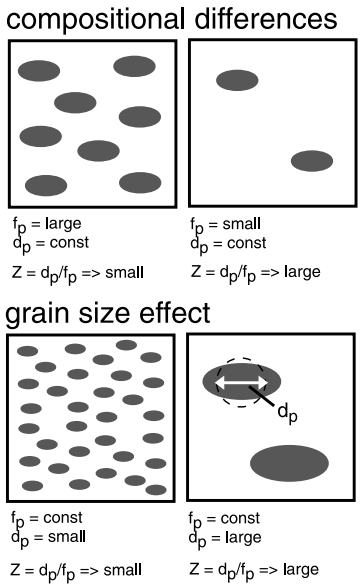

Fig. 3. Variations of the Zener parameter (Z) for changes in volume (top row) or size (bottom row) of second-phases. d_p: second-phase diameter, f_p: second-phase volume fraction.

4.4. Influence of temperature

To investigate the effect of temperature on microstructural changes, we have to compare between samples

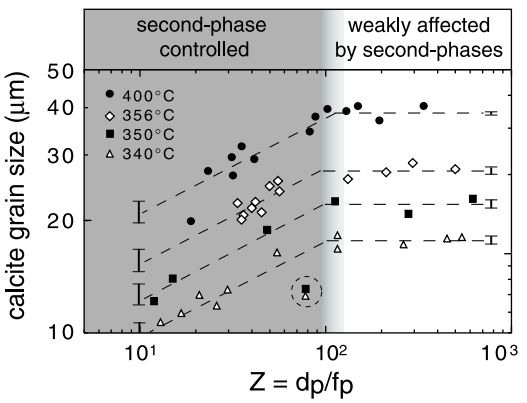

Fig. 4. Zener parameter vs. calcite grain size for samples at different temperatures (340 °C: triangles, 350 °C: squares, 356 °C: rhombs, 400 °C: circles). Error bars in mean grain size of calcite given for second-phase controlled microfabrics and microfabrics weakly affected by second-phases. Regression line of second-phase controlled microstructures is derived by Eq. (2) using an average $m*$ of 0.25 (see Table 2).

deformed at different temperatures but with similar Zener parameter. Note that the facts that all samples derive from the same thrust plane and were deformed simultaneously during thrusting imply an identical strain rate for the different locations.

With increasing temperature, the average size of the matrix calcite increases in a way that the grain size differences between the curves correlate with the measured relative temperature differences between the individual locations. For all temperatures, the two aforementioned microstructure types persist. In the case of second-phase controlled microfabrics, regression of Eq. (2) yields similar slopes for different temperatures resulting in a mean value for $m*$ of 0.25 ± 0.03 (see Table 2 and Fig. 4). Note that due to data clustering samples deformed at 356 °C were excluded for calculation of $m*$. Furthermore, two outliers at $Z \sim 80$ (sample deformed at 340 and 350°C; see dashed circle in Fig. 4) were excluded for the calculations because they represent most likely microstructures related to a localized late deformational overprint. For microstructures that are weakly affected by second-phases, the calcite grain size corresponds to d_g for $Z = 100$ (Eq. (2)) and remains constant with increasing Z. The average error in d_g in this microstructure type is ±2.1%. Based on the data available, it is debatable whether the transition of both microstructure types is abrupt or rather gradual (Fig. 4). As a first approximation, however, the aforementioned treatment seems to be appropriate. Besides mean grain size, knowledge about the grain size distribution is another important factor to be considered, because in a grain aggregate different deformation mechanisms can occur in different grain size classes (e.g. Heilbronner and Bruhn, 1999; ter Heege, 2002). Grain size distributions for low and high temperature and both high and low Zener parameters are unimodal but the grain size range is larger for samples with high Zener parameter (Fig. 5). The standard deviations as a measure of the grain size distributions follow the trends already manifest by the mean grain sizes. In logarithmic space, the distributions for all Zener parameters are close to log-normal and show only a slight negative skewness. The elongation of calcite grains as an additional microstructural feature increases from 0.55–0.65 to 0.3–0.4 with decreasing Z (Fig. 6). The decrease is more pronounced in microstructures that are weakly affected by second-phases. Furthermore, the data suggest a tendency for enhanced grain elongation with increasing temperature at constant Z.

Table 2
Errors and fit quality (R) for regressions after Eq. (2) for second-phase controlled microstructures of Fig. 4

Temperature (°C)	c	m*	R
400	10.69 ± 1.58	0.27 ± 0.04	0.94
356	2.57 ± 1.29	0.57 ± 0.13	0.54
350	6.84 ± 0.58	0.25 ± 0.02	0.99
340	6.05 ± 0.62	0.23 ± 0.03	0.96

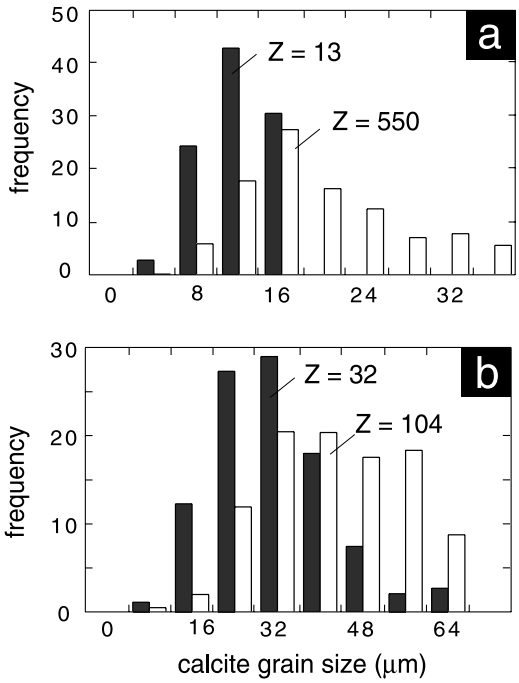

Fig. 5. Characteristic grain size distribution histograms of calcite for microfabrics with high (white bars) and low Zener (black bars) parameter. Grain size data in (a) and (b) derive from samples deformed at 340 and 400 °C, respectively.

The calcite–calcite grain boundary fraction decreases for all samples more in the second-phase controlled part than in the second-phase unaffected one (Fig. 7) resulting in ranges of 0.4–0.9 and 0.8–1.0 for calcite grain boundary fractions, respectively. As documented above, the Zener parameter comprises information about both volume and size of second-phases. In order to unravel the influence of the individual parameters, Fig. 8 shows the changes of the calcite–calcite grain boundary fraction as a function of the second-phase volume proportion. It becomes evident that with increasing second-phase content the calcite–calcite grain boundary and the interface fractions, respectively, decrease and increase in a dramatic manner. In this way, only 9 vol% of second-phase particles are required to reduce

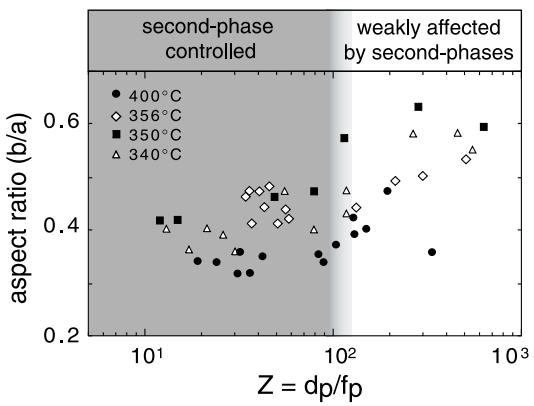

Fig. 6. Changes in the calcite aspect ratio (minor/major axis) in dependence of the Zener parameter for all samples. Symbols are identical to Fig. 4.

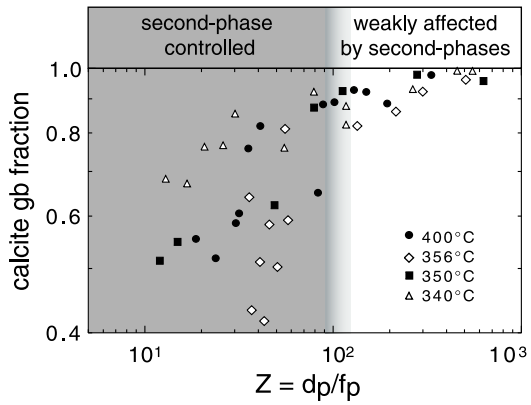

Fig. 7. Changes of the calcite grain boundary fraction as function of the Zener parameter at different temperatures (same samples and symbols as in Fig. 4).

the calcite–calcite grain boundary fraction to 0.5. In addition, these changes seem to be similar for the different samples and therefore show only a weak temperature-dependence in the temperature range investigated.

4.5. Crystallographic preferred orientation (CPO)

In order to check for potential influences of the second-phases on CPO, textural analysis was performed on microfabrics with different calcite grain size, i.e. Zener parameter, for the sample deformed at 400 °C. With increasing Z the texture intensity increases and c-axis distribution changes (Fig. 9). Typical c-axis point maxima exist for the pure samples but these maxima become more and more smeared out with decreasing Z tending towards a random c-axis pattern. Both trends point towards a CPO weakening with decreasing Zener parameter. This is in excellent agreement with EBSD investigations by Burlini and Kunze (2000) performed on carbonate mylonites with zero and 5 vol% of second-phases, which show a CPO for the pure sample, while a random distribution dominates in the impure one. More recently, Krabbendam et al. (2003) observed a similar textural change from pure quartz

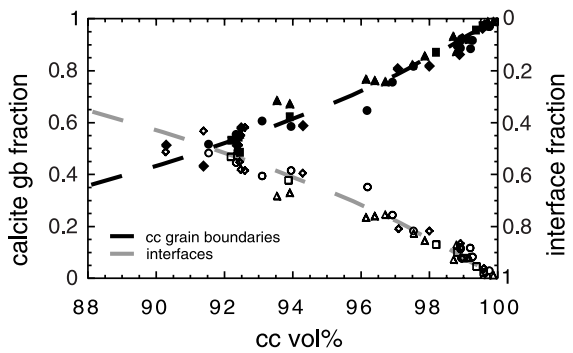

Fig. 8. Changes of the calcite grain boundary and interface fraction as a function of the calcite volume % (same samples and symbols as in Fig. 4).

mylonites towards impure ones with dispersed graphite as second-phase mineral.

5. The cause of the Zener parameter dependent microstructural changes

The relationship between Zener parameter and calcite grain size indicates that the grain sizes in all layers are stabilized (Fig. 4) and indeed represent steady-state microstructures. With increasing temperature, the grain size stabilization persists but results in a shift towards larger average calcite grain sizes. Based on the microstructural and textural characterizations presented above, two general microfabrics have to be distinguished (see Figs. 4–7 and 9). (a) Second-phase controlled microfabrics show a continuous increase in calcite grain size, calcite grain boundary fraction and strengthening in CPO with increasing Zener parameter. (b) The first two features (Figs. 4 and 7) define the transitions towards calcite microfabrics that are only weakly affected by the second-phases. This microstructure type is characterized by constant calcite mean grain sizes, a gentler increase in calcite grain boundary fraction and a higher texture intensity (Fig. 9). In light of deformation mechanisms, the reduction in grain size, the weakening of CPO and the drastic increase in the interface fraction with decreasing Zener parameter points to a change in the predominant deformation mechanism from dislocation creep towards second-phase controlled granular flow. Similar changes in deformation mechanisms were previously suggested for pure and impure mylonites by Olgaard (1990), Burlini and Kunze (2000) and Krabbendam et al. (2003). The major new facts discovered in our sample suite are: (a) the abrupt change between the two microfabric types, and (b) the temperature-dependence of the relationship Z versus calcite grain size (Fig. 4). Both points can be explained in terms of differences in the mechanisms involved in grain size stabilization and their temperature-dependent evolution.

(a) In general, steady state grain sizes in a pure monomineralic mylonite are preserved by a balance of grain size increasing and decreasing mechanisms and represent therefore a rather dynamic state (Means, 1981; Herwegh et al., 1997; Shimizu, 1998; de Bresser et al., 2001; Pieri et al., 2001). While subgrain rotation recrystallization, bulging nucleation and classical nucleation can induce grain size reduction (e.g. Drury and Urai, 1990), syndeformational grain growth is the predominant coarsening process. The latter requires grain boundary migration recrystallization, i.e. mobile grain boundaries. In this sense the grain boundary mobility depends on the driving forces, which basically are surface energy and/or the internal stored energy. It is well known that surface energy is the major driving force for grain growth under static conditions and probably also plays an important role during syndeformational grain growth for small grain sizes. However, it is

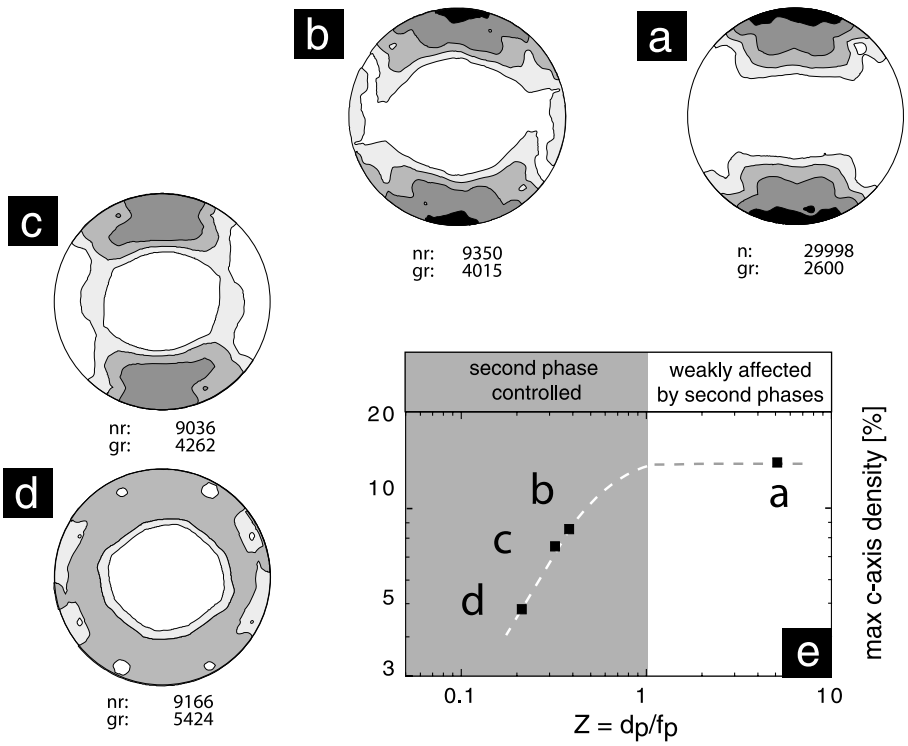

Fig. 9. Textural changes as function of the Zener parameter for sample deformed at 400 °C. (a)–(d) Contoured *c*-axes stereographic projections (contour intervals are 1, 2, 4… times uniform distribution), (e) diagram shows maximum *c*-axis density vs. *Z*.

unclear yet, if under natural conditions, internal stored energy contributes to grain growth or just enhances the grain boundary mobility without having any major grain growth component. In the context of grain size stabilization, where individual grains are continuously subjected to grain growth or grain size reduction, stabilization via dynamic recrystallization is suggested. In contrast, for second-phase controlled microfabrics a considerable part of calcite grain boundaries is pinned due to the high interface fraction (Fig. 8) and therefore many grain boundaries are immobile resulting in grain size stabilization (Fig. 4). Thus, the calcite grain size is related to the size and volume fraction of the second-phases via Eq. (2). As a consequence of pinned grain boundaries, recovery of the microfabric via grain boundary migration becomes strongly reduced resulting in weak CPOs (Fig. 9). Therefore, we interpret that deformation via granular flow predominates in second-phase-controlled microfabrics (Paterson, 1995). For this deformation mechanism, grain boundary sliding and mass transfer are the major strain accommodation processes but a less pronounced contribution of dislocation creep might still be possible. The occurrence of weak CPOs confirms the latter point while the drastic increase in interface fraction and the alignments of sheet silicates (see Fig. 2 and Herwegh and Jenni, 2001) imply a major contribution of grain boundary sliding. In terms of mass transfer, Herwegh and Jenni (2001) were able to show for the same samples that sheet silicates undergo cycles of shrinkage and growth due to a combination of dissolution, mass transfer, nucleation and precipitation. For calcite, no unique criterion for the detection of mass transfer exists but based on the sheet silicate observations, this process is very likely to occur as well. The strong elongation observed in calcite grains in second-phase controlled microfabrics might therefore represent an additional hint in this direction because anisotropic grain growth by mass transfer is one way to explain enhanced grain elongations (see Karato and Masuda, 1989). In contrast, deformation by intracrystalline plasticity is the classical way to generate elongate grain shapes. With respect to these two possibilities, we cannot be conclusive but the weak CPOs at least indicate that dynamic recrystallization via grain boundary migration is unable to strengthen the texture. Thus, the alternative way to recover the internally stored energy in a grain has to go via dissolution, mass transfer and precipitation processes.

(b) With increasing temperature, both second-phase controlled and weakly affected microfabrics show an increased stabilized calcite grain size implying that coarsening is related to different processes. While increasing temperature will enhance the grain boundary mobility and therefore the grain growth component in microstructures weakly affected by second-phases, the grain growth in second-phase controlled microstructures can be explained by two hypotheses. (a) Due to higher grain boundary mobilities, second-phases can be dragged over larger distances. (b) Temperature enhanced grain growth of the second-phases. In this way the average grain size of sheet silicates still increases but their number fraction per unit

area decreases. Hence, the average distance between the individual second-phase particles must become larger and therefore the calcite grains can grow until they become pinned. The recrystallization cycles of second-phases are a function of temperature and time. In this way, the nucleation rate of new particles together with the grain growth kinetics of the second-phase particles can directly control the grain size of the matrix mineral. As will be shown below, these two hypotheses can be reinvestigated on the base of an energy-based modeling.

In summary, the stabilized grain sizes vary as a function of the content and size of second-phases in the calcite mylonite resulting in static and dynamic grain size stabilization manifest by pinning/dragging and by a combination of second-phase dragging and dynamic recrystallization, respectively. As a consequence, a switch from granular flow to dislocation creep dominated flow occurs. Although based on quantified microstructural arguments this statement is of qualitative nature only, a fact that is valid for many microstructural investigations on natural samples. In the following we therefore outline an energy-based concept, which represents an attempt to investigate the influence of second-phase minerals on the processes involved in deformation in a more quantitative manner.

6. A microstructure-based energy concept

Based on Zener drag induced microstructural variations, we develop in this chapter a concept for the quantification of deformation processes. In this context, we use the balance of different microfabric modifying processes, which are activated to maintain dynamic steady state deformation of an aggregate, and define an internal energy term for each process. It is important to note that this concept deviates from classical thermodynamic approaches because the definition of the internal energy terms is based on the microstructure. Furthermore, the energy terms presented below always relate to a steady state bulk microstructure and not to local energy states in the microfabric. Finally, we have to point out that the concept does not investigate the energy transfer in the material in a continuum mechanical sense, which would require energy determination at given stress and strain rate states.

In order to compare the different energies between each other and to detect their variations for different physical conditions, both microstructural parameters and energies have to be related to a unit volume. Stereology theory shows that 2-D quantification in many cases is sufficient for the description of a 3-D fabric (Underwood, 1970). Moreover, 2-D cuts represent the most common space for geological investigations as intensively done in the case of thin or polished sections. Therefore, all microstructural data are normalized per unit area (m^2), the energies are given per m^2 and they have the unit J/m^2 at constant T, σ, $\dot{\epsilon}$.

The total free energy of a system at given external conditions (temperature (T), confining pressure (P_c) including differential stresses (σ) and strain rate ($\dot{\epsilon}$)), can be considered as a sum of different free energies (Cumbest et al., 1989; Stünitz, 1998):

$$G^{\mathrm{tot}}_{T,\,\sigma,\,\dot{\epsilon}} = G_{\mathrm{chem}} + G_{\mathrm{fabric}} + G_{\mathrm{elast}} \tag{3}$$

where G_{chem} describes the free energy of a given chemical system, G_{fabric} is related to a steady state fabric and G_{elast} is the elastic lattice distortion due to external stresses. G_{elast} can be neglected in plastic deformation because all elastic proportions are relaxed without any stresses (Paterson, 1973; Poirier, 1985). Energy of any defined chemical system (G_{chem}) predicts the stable mineral assemblage for the particular conditions. The samples investigated in this study are assumed to be chemically equilibrated and ΔG_{chem} is zero. As a consequence, Eq. (3) is dominated by G_{fabric} as the remaining energy term, which in the following will be discussed for steady state microfabrics. Principally, four major types of energy control a microfabric at a given temperature (T), pressure (P) and strain rate ($\dot{\epsilon}$), surface energies (G_{surf}), dragging energies (G_{drag}) and energies related to the deformation mechanisms, i.e. dislocation creep energy (G_{dcr}) and granular flow or diffusion creep energy (G_{grf}):

$$G_{\mathrm{fabric}\ (T,\,\sigma,\,\dot{\epsilon})} = G_{\mathrm{surf}} + G_{\mathrm{drag}} + G_{\mathrm{dcr}} + G_{\mathrm{grf}} \tag{4}$$

In terms of microstructure modifications, diffusion creep or granular flow induces no or only weak microstructural changes (Schmid et al., 1977; Schmid and Handy, 1991) and as a first approximation this energy part of the system is therefore assumed to be close to zero (see also paragraph before). In contrast, dislocation creep changes free energy by stored dislocations or the generation of new low and high angle grain boundaries. In the microfabrics the interplay between these energies is manifest by variable values for different microstructural parameters (see below).

6.1. Surface energy

The energy of any material-surface is an intrinsic value (Spry, 1969; Kretz, 1994). The minimization of this surface energy is the driving force for grain-growth under chemically equilibrated conditions (Evans et al., 2001). Particularly for fine-grained mylonites, surface energy might significantly contribute to syndeformational grain growth as well. The surface energy (J/m^2) per unit area can be calculated by:

$$G_{\mathrm{surf}} = \gamma_{\mathrm{A}} s_{\mathrm{g}} \tag{5}$$

where γ_{A} (J/m) is the tension energy and s_{g} (m/m^2) is the total length of grain boundaries per unit area. In detail, γ_{A} varies not only between different minerals but also with the orientation of a grain boundary with respect to the crystallographic directions of an individual crystal. For most

crystal systems, these differences are small but it would be appropriate to either give γ_A as an average of the different crystallographic directions or resolve it specifically in dependence of the crystallographic misorientation between two neighbor grains. Data for both approaches are not available yet. Besides the crystallographic dependence, the exact value of γ_A varies between different studies, but γ_A has always the same order of magnitude (Spry, 1969). In light of Eq. (5), however, the microstructural variations in s_g are 4–5 orders of magnitude larger than the error in γ_A, which is somewhere between 0.1 and 0.5. Therefore, the total length of grain boundaries per unit area will be the important parameter to discuss in the context of the bulk surface energy of a mylonite.

6.2. Dragging energy

In pure monophase mylonites the surface energies are responsible for grain growth. In contrast, second-phase minerals in polyphase mylonites will hinder grain growth by dragging or pinning the grain boundaries of the matrix mineral requiring an energy term that we call dragging energy. In the past, different approaches have been developed to calculate the dragging force induced on a grain boundary by an individual second-phase particle (see references in Evans et al., 2001 and their fig. 4). For this study, we choose the formulation after Ryum et al. (1983) because it integrates the shape of the particles in the calculation of the dragging force (F^{p}_{drag}):

$$F^{p}_{drag} = \pi d_p \gamma \left(\frac{1}{(1+E_p)E_p^{1/3}} \right) \tag{6}$$

where d_p is the size of the second-phase (in m) and E_p is the dimensionless ellipsity of the second-phase particle. Eq. (6) suggests that the dragging force induced by a single particle primarily depends on its size and only to a minor extend on its shape. Note that this point is debatable because particularly sheet silicates, i.e. strongly anisotropic grains, seem to have in nature more influence on moving grain boundaries than spherical ones (e.g. Voll, 1961). At the present stage of knowledge, however, we have to rely on Eq. (6). In order to obtain the total dragging force (F^{tot}_{drag}) induced by the particles per unit area, F^{p}_{drag} has to be multiplied by the number (n_p) of second-phases per unit area:

$$F^{tot}_{drag} = F^{p}_{drag} n_p \tag{7}$$

The energy is defined by force times distance. Transferred to our system, we therefore suggest that the total energy (G_{drag}) required to overcome F^{tot}_{drag} of the system per unit can be expressed by:

$$G_{drag} = F^{tot}_{drag} L^{tot}_{p} \tag{8}$$

L^{tot}_{p} is the sum of all the dragging distances per unit area, which can be calculated by:

$$L^{tot}_{p} = L n_p \tag{9}$$

The dragging distance L (in m) of the individual second-phase particle is an unknown parameter in our system. As discussed below, however, we can estimate a first order approximation reflected by an upper (grain size of matrix mineral) and lower (minor axis of second-phase mineral) bound for L.

6.3. Dislocation creep energy

Any material deforming by intracrystalline plasticity stores at least a part of the deformation energy in the form of internal energy. In mylonites this stored internal energy is manifest by the density of their lattice defects like screw and edge dislocations (Stünitz, 1998). After Hull and Bacon (1984), the energy of screw dislocations can be calculated by:

$$E = \left(\frac{\mu b^2}{4\pi} \right) \ln\left(\frac{R}{r_0} \right) + \alpha \mu b^2 \tag{10a}$$

where μ is the shear modulus, b the burgers vector, R the outer radius of the volume around the dislocation, r_0 the inner radius around the dislocation; and an α factor between 0.3 and 0.5 (Hull and Bacon, 1984). Up to now, the knowledge of r_0 and the core energy of a dislocation has been limited to some highly symmetric minerals and alloys (Schoeck, 1995). In the absence of exact values for calcite, $r_0 = 5b$ as the size of the dislocation core is used following the approximation by Wertmann and Wertmann (1992) (see also Stünitz, 1998). Equivalent to this formulation, the energy of an edge dislocation can also be calculated from:

$$E = \left(\frac{\mu b^2}{4\pi(1-\nu)} \right) \ln\left(\frac{R}{r_0} \right) + \alpha \mu b^2 \tag{10b}$$

where additionally the Poissons ratio (ν) is necessary. Multiplying the energy of one dislocation (J) with dislocation density (D_{dis}), we receive the internal strain energy per unit volume (Jm/m^3). We transfer these in two dimensions by an exponent of $^{2/3}$ to known dislocation densities.

$$G_{dcr} = E D_{dis} \tag{11}$$

The energy difference between screw- and edge-dislocations is very limited, but the dislocation densities may vary by several orders of magnitude (Christie and Ardell, 1976; Nicolas and Poirier, 1976; White, 1977). This density depends on the relative importance of dislocation glide and creep versus the recovery behavior of the material during deformation.

From a microstructural point of view the dislocation energy, i.e. the differences in dislocation density across grain boundaries, acts as the driving force for grain boundary migration recrystallization, which reduces differences in

internal stored energy via recovery. In this way, the dislocation energy could also act as an additional driving force for grain growth and therefore two different scenarios have to be considered. (a) Averaged over the entire sample, the internal stored energy formed per strain increment becomes recovered via grain boundary migration at the same rate as dislocation formation takes place. Although the grain boundaries are locally sweeping in the microstructure all the time, integrated over the entire sample, no deformation induced grain growth component would be expected at constant physical conditions. (b) In the case that dislocations generate faster than they become recovered, deformation induced grain growth will take place. As already mentioned above, insufficient information is available so far to be conclusive with respect to a deformation induced grain growth component. In the context of this study, therefore, we restrict ourselves to case (a). However, we are aware that under the presence of deformation induced grain growth an additional energy term for deformation induced grain growth would be required.

In summary, the proposed energies are connected to measurable values, which can be obtained directly from the microfabrics. As a great advantage of this energetic approach the dimensions of microstructural parameters like number of second-phase particles or total grain boundary length per unit area represent clearly the predominating factors in all three energy calculations. In other words, all parameters that cannot directly be derived from the microstructure and therefore might be subjected to a certain degree of uncertainty (e.g. γ or D_{dis}) are of subordinate importance as long as their variability is restricted within a range smaller than one order of magnitude. Finally, the consideration requires a steady state microfabric and an equilibration of chemical energies (Stünitz, 1998). Interaction between chemical and fabric energies should be possible to handle in the concept, but will not be discussed in this example.

7. The energy concept applied to steady state fabrics in nature

To unravel the influence of the second-phase particles on the different energies, we present first the energy considerations for the sample deformed at 350 °C, i.e. for microstructures that have developed at constant temperature but variable second-phase content (see above). Based on all samples investigated the temperature dependent energy changes will be discussed afterwards.

7.1. Constant temperature

In order to solve Eq. (5) the required parameter s_g can be obtained via microstructural analysis. For the $10\bar{1}1$ face in calcite, Spry (1969) gives a list of γ_A that ranges from 0.078 to 1. For our study we choose the γ_A value of 0.23 (Gilman, 1960), which is based on experiments and close to his theoretical considerations ($\gamma_A = 0.19$). The bold line in Fig. 10 shows the calculated surface energies of the matrix calcite grains as a function of the Zener parameter. With increasing Zener parameter, i.e. calcite grain size, the surface energy decreases (Spry, 1969).

Dragging forces for individual parameters are calculated after Eq. (6) for each second-phase particle taking then the mean value of the derived data. The parameters d_g, d_p, f_p and E_p derived directly from image analysis of the microstructures while for γ_A again the value of Gilman (1960) was taken. For the estimation of the dragging energy (Eqs. (6)–(9)) the dragging distance L is an unknown parameter. However, as a first approximation we chose the second-phase's minor axis and the calcite grain size. Similar to the surface energy, also the dragging energy decreases with increasing Zener parameter (Fig. 10a) but in a much more pronounced way. For the different dragging distances, the slope remains constant and shifts towards higher energy values with increasing L. Recalling the subdivision in second-phase controlled and microstructures that are weakly affected by second-phase (Figs. 4–7), the microstructural

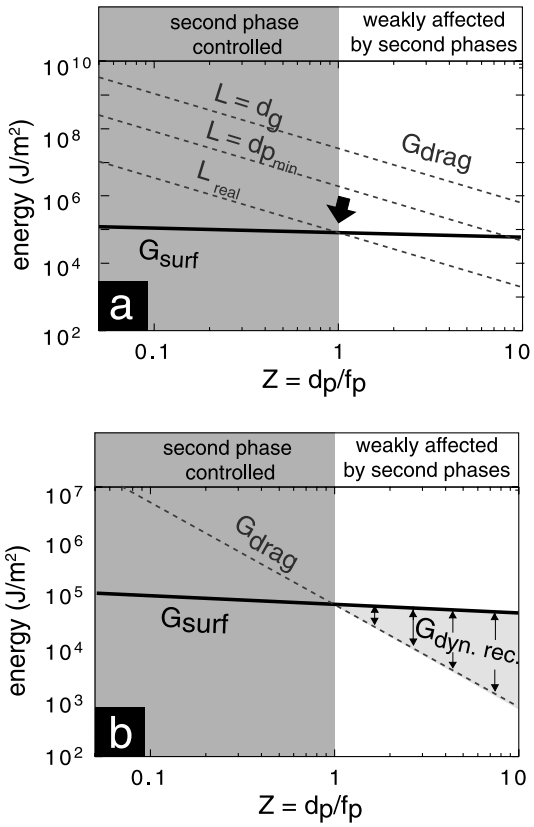

Fig. 10. (a) Changes of surface (Eq. (5)) and dragging (Eqs. (6)–(9)) energy as function of the Zener parameter at constant temperature (350 °C). Dragging energies are calculated for two different dragging lengths (L): (1) average minor axis of second-phases (d_p^{min}), (2) calcite grain size (d_g). L_{real} is obtained by shifting the calculated dragging energy curves onto the intersection of surface energy and microstructure transition ($Z = 100$). (b) For $Z > 100$ the difference between surface energy and dragging energy is proportional to the dynamic recrystallization energy.

change in slope (Fig. 4) must also be manifest in changes of the system's energy. In this sense, dragging energies higher than surface energies means that grain coarsening of the matrix mineral is prevented, i.e. the matrix grains are pinned by the second-phase. In contrast, surface energies higher than dragging energies should be manifest in the growth of the matrix minerals. Keeping these relationships in mind we suggest that the two energies should cross each other exactly at $Z = 100$ allowing grain size stabilization of the matrix mineral by the second-phases for all Zener parameters smaller than 100. For that reason we can shift the curve of the dragging energy through the d_p/f_p value of the slope break and the corresponding surface energy (Fig. 10a).

For Z larger than 100, the dragging energy is too low to solely maintain a constant grain size by counteracting the surface energy. From a microstructural point of view, however, the grain sizes are stabilized, i.e. the grains do not continuously grow, suggesting dynamic recrystallization as additional grain size reducing process. This process also requires energy and we therefore suggest the difference between surface and dragging energy to reflect the dynamic recrystallization energy (Fig. 10b). Using the presented approach, we are aware that any crystallography induced contribution is not incorporated yet (e.g. Kruhl, 2001; Kruhl and Peternell, 2002). Before such integration is possible, detailed quantitative work on the role of crystallographic misorientations on grain boundary migration is required.

All energies obtained by the energy concept are related to each other and can therefore at least be used in a relative manner enabling us to gain energy estimations directly from the sample. However, how realistic are the obtained energies in an absolute sense? No independent evaluation method exists for the dragging energy and surface energy but the dynamic recrystallization energy is directly related to the dislocation creep energy, i.e. the generation of dislocations as a function of the ambient conditions of deformation. Applying Eqs. (10a), (10b) and (11), we can estimate the latter for pure calcite by calculating the energy of a screw dislocation in the ⟨r⟩ glide system (a main glide system in calcite). This simplification is appropriate because the differences between ⟨r⟩ and ⟨f⟩ as major glide systems in calcite are very small and vary only by 1.7 Å in the Burgers vector of the two glide systems (8.09 Å vs. 6.37 Å). Fig. 11 shows the resulting energies for a 2-D unit area as function of the dislocation density (see also Stünitz, 1998). In log–log space, the dislocation energies increase continuously with increasing dislocation densities. The horizontal black bar in Fig. 11 presents the range of our calculated dynamic recrystallization energies for Zener parameters of 500, i.e. relatively pure calcite mylonites, implying dislocation densities around $10^{12}\,m^{-2}$. Dislocation densities in fine grained natural mylonites (1–10 μm) from the Helvetic Alps (Pfiffner, 1982) and the Tutt shear zone in South Wales (de Bresser, 1991), which were deformed at 350 and 200 °C, show dislocation densities of $4.4–5.7 \times 10^{13}\,m^{-2}$ and $2.5 \times 10^{13}\,m^{-2}$, respectively (see 1 and 2 in Fig. 11).

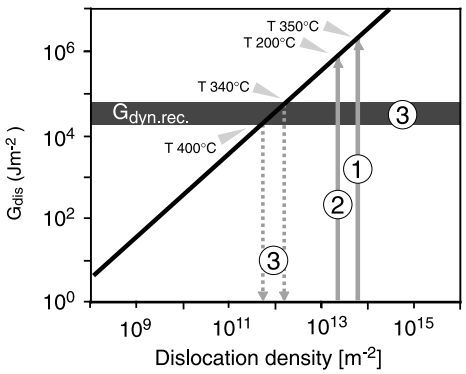

Fig. 11. Solid line shows changes in dislocation energy (G_{dis}) per unit area as function of dislocation density. Based on Eqs. (10a) and (11), screw dislocations in ⟨f⟩-direction in calcite (Burgers-vector: 6.37 Å; shear modulus 32 GPa,) are used for the calculation. Solid vertical lines indicate dislocation densities observed in natural carbonate mylonites (1: Pfiffner, 1982 and 2: de Bresser, 1991). Horizontal back bar (3) covers the range obtained for dynamic recrystallization energy (see also Fig. 10) predicting dislocation densities of about $10^{12}\,m^{-2}$ (3).

Hence, there is a discrepancy between energies calculated from dislocation densities of natural samples and the dynamic recrystallization energy obtained by our approach of about 1–1.5 orders of magnitude. Keeping in mind, however, (a) that exhumation processes can artificially enhance dislocation densities of natural samples and (b) that in terms of temperature the data of de Bresser (1991) present the low temperature continuation of our prediction (compare 2 and 3 in Fig. 11), the obtained data might be in the correct order of magnitude. An alternative explanation for the discrepancy might be based on a potential influence of strain induced grain growth unknown and therefore not incorporated so far. In this way, higher energies would occur than predicted at the present stage. In summary, the energy concept might be valid in terms of absolute values but more work is required to confirm this point.

7.2. Temperature dependence

The relations between Zener parameter versus the system's energy can be expanded in a third dimension by incorporating temperature (cf Figs. 10 and 12). In this 3-D space different 2-D cuts can be presented as a temperature versus energy diagram (Fig. 12a). Fig. 12b–d shows log T–log G diagrams at Zener parameters of 10 (strong second-phase controlled microstructures), at Zener parameter of the change in slope ($Z = 100$) and Zener parameter of 500 (relatively pure mylonites). In general the total energy of the considered term, dragging energy, surface energy and dynamic recrystallization energy decrease with increasing temperature. At Zener parameters of 10 the dragging energies are not only higher than the surface energies in the corresponding sample but also higher with respect to the surface energies of all other samples. In other words, for low Zener parameters the second-phase particles cannot be dragged because of a too low surface energy with respect to

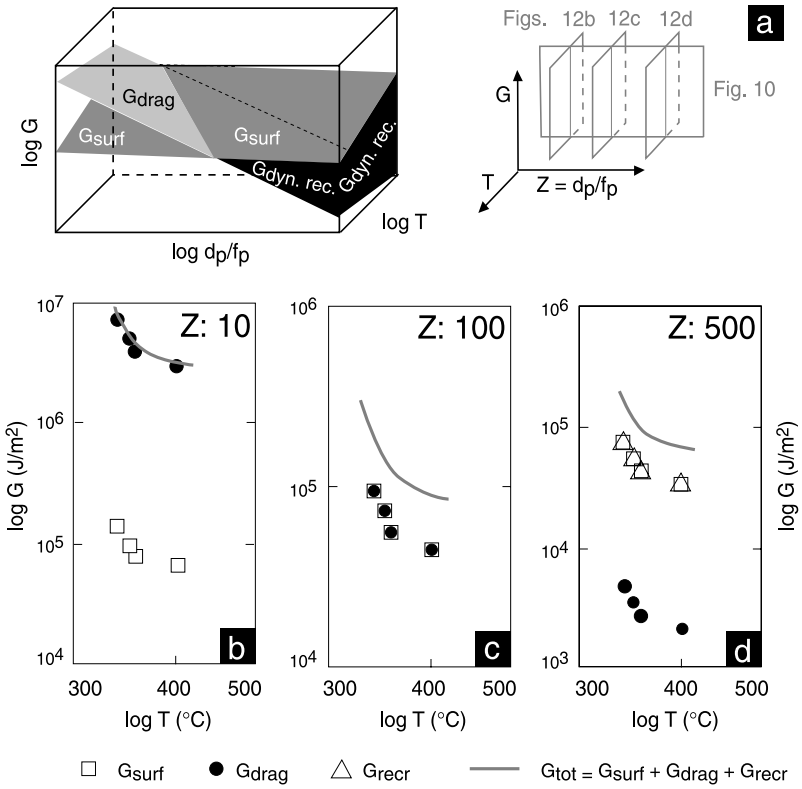

Fig. 12. Temperature dependent energy variations: (a) Schematic block diagram of the space Zener parameter (Z), energy (G) and temperature (right) and the corresponding sections (left) shown in ((b)–(d)). Energies against temperature at constant Z ((b)–(d)).

the dragging energy. Hence, the calcite grain boundaries must be pinned. Revisiting the discussion about temperature-dependent pinning, this implication allows the exclusion of the long-distance dragging hypothesis. As a consequence, second-phase coarsening must reflect the grain size stabilization parameter for the matrix calcite in second-phase-controlled microstructures.

7.3. The energy concept in the context of microstructural evolution

On the way to a steady state fabric, grain size and CPO (crystallographic preferred orientation) evolve as a function of increasing shear strain approaching characteristic microfabrics. Their microstructural and textural parameters depend on the physical conditions of deformation and the intrinsic material properties. The grain size, for example, has to increase and decrease, respectively, for initial grain sizes too small and too large in the host rock. In our system of carbonate mylonites, pure and initially coarse grained vein calcites show a grain size reduction while a grain size increase has to be expected for the initially micritic impure calcite. Based on the energy concept, this behavior can again be seen as an energy minimization process of the entire system (Fig. 13). For this purpose we have to address the energy changes (vertical axis) as a function of Zener parameter times average calcite grain size ($Z{\cdot}d_g$, horizontal axis). While the dragging and surface energy decrease from low to high $Z{\cdot}d_g$ values, the opposite trend is manifest by the dynamic recrystallization energy. Thus the total system approaches an energy minimum at moderate $Z{\cdot}d_g$ values, which corresponds to the steady state grains size at given T, σ, $\dot{\epsilon}$. As already seen in Fig. 12c and d, the point of minimum total energy will shift towards lower values with increasing temperature.

8. Concluding remarks and perspectives for future investigations

The fact that with decreasing Zener parameter the texture weakens and both calcite grain size and the free mobile calcite grain boundaries decrease indicates that less calcite–calcite grain boundaries are able to recover the internally stored energy by dynamic recrystallization. For that reason, a gradual transition from dislocation creep to granular flow dominated deformation has to occur between second-phase controlled microfabrics and microfabrics only weakly affected by second-phases. This is in agreement with previous studies (e.g. Olgaard, 1990; Burlini and Kunze, 2000; Krabbendam et al., 2003). The inference about this switch in deformation mechanism has several important implications for the interpretation of polymineralic mylonites:

(a) As outlined above, the parallel geometry in combination with invariant thickness of the layers with

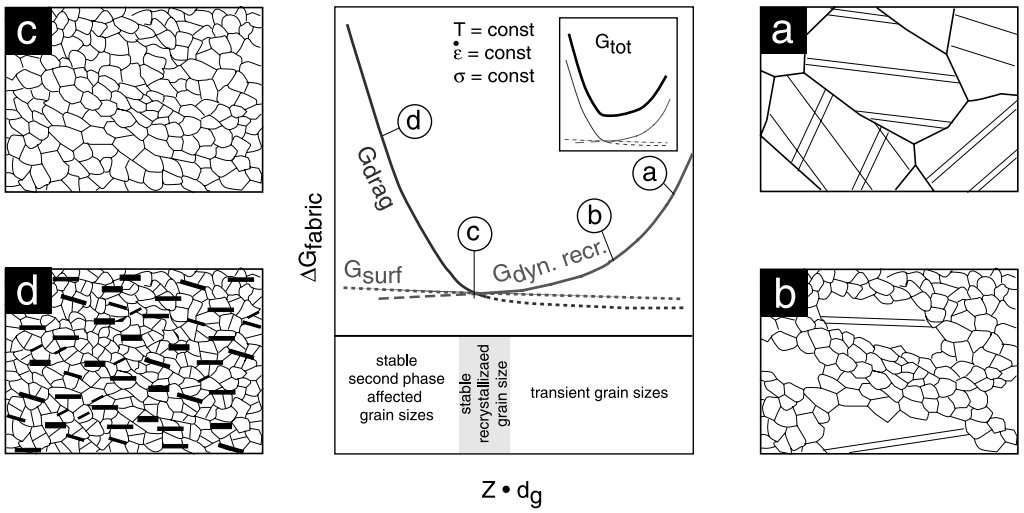

Fig. 13. Energy minimization during microfabric evolution shown as function of the Zener parameter (Z) times the matrix grains size (d_g).

different second-phase contents implies homogeneous deformation, i.e. a similar viscosity and therefore similar strain rate and stress states for the different layers. The preservation of the equiviscous point in a polymineralic system is only possible when the contributions of the major deformation mechanisms varies and this is exactly what can be inferred from the microstructural variability observed in our natural carbonate mylonites. Thus, both microfabric and the interplay of granular flow and dislocation creep as major deformation mechanisms are adjusted as a function of the second-phases grain size and volume proportion such that homogeneous deformation becomes possible.

(b) Based on the calculation of the dynamic recrystallization energy it might be possible to quantitatively investigate the transition from dislocation creep to granular flow because the latter is the counteracting process to dislocation creep during deformation (de Bresser et al., 2001).

(c) In light of natural microstructures, the presented concept can be applied to different crustal sections and mineral systems (e.g. quartz-sheet silicates, olivine–enstatite) to quantitatively investigate the influence of temperature, strain rate and stress states on the deformation mechanism.

(d) Furthermore the presented concepts could provide new insights into grain growth and paleopiezometry in polymineralic systems.

(e) The energy concepts could be expanded towards a powerful tool to connect microstructural energies with chemical variations in polymineralic systems.

In light of future perspectives, incorporation of the effect of crystallographic misorientations and shapes of second-phases on grain boundary migration of the matrix mineral would provide further improvements of the present stage. Of special note in this context is the role of strain energy on grain growth because, if important, the obtained dynamic recrystallization energies would shift towards higher values.

Giving a great advantage, the energy concept is able to link quantified microstructural changes with the associated processes. For that reason, the approach is applicable to both naturally and experimentally deformed polymineralic mylonites, providing a great opportunity to compare both systems with each other. In this way, the role of competing processes responsible for microstructure stabilization and detections of potential differences between nature and experiment are possible in future studies.

Acknowledgements

Up to the present state of this work, we benefited from numerous stimulating discussions with colleagues from different research disciplines. In this context, we would like to particularly thank the participants of the Bern–Basel petro-seminar for their positive criticism and feedback. G. Schreurs is acknowledged for reviewing an earlier version of this manuscript. The manuscript was significantly improved by the reviews of J. Kruhl and A. Krohe as well as by editorial handling of J. Hippertt. Last but not least we would like to thank Rod Holcomb and Frank Fueten for providing GEOrient and GV, respectively. M. Herwegh acknowledges financial support by Swiss National Science Foundation (SNF project: 2100-066889).

References

Bestmann, M., Kunze, K., Matthews, A., 2000. Evolution of a calcite marble shear zone complex on Thassos Island, Greece: microstructural and textural fabrics and their kinematic significance. Journal of Structural Geology 22, 1789–1807.

Bruhn, D.F., Olgaard, D.L., Dell'Angelo, L.N., 1999. Evidence for enhanced deformation in two-phase rocks: experiments on the rheology

of calcite–anhydrite aggregates. Journal of Geophysical Research 104, 707–724.
Burkhard, M., 1988. L'Helvetique de la bordure occidentale du massif de l'Aar (évolution tectonique et métamorphique). Eclogae Geologicae Helvetiae 81, 63–114.
Burlini, L., Kunze, K., 2000. Fabric and seismic properties of Carrara marble mylonite. Physics and Chemistry of the Earth 25, 133–139.
Christie, J.M., Ardell, A.J., 1976. Deformation structures in minerals. In: Wenk, H.-R., (Ed.), Electron Microscopy in Minerals, Springer, Berlin, Heidelberg, New York, pp. 373–403.
Cumbest, R.J., Drury, M.R., van Roermund, H.L.M., Simpson, C., 1989. Dynamic recrystallization and chemical evolution of clinoamphibole from Senja Norway. Contributions to Mineralogy and Petrology 101, 339–349.
de Bresser, J.H.P., 1991. Intracrystalline deformation of calcite, Geologica Ultraiectina, 79 (PhD thesis, Rijksuniversiteit, Utrecht).
de Bresser, J.H.P., Peach, C., Reijs, J., Spiers, C.J., 1998. On dynamic recrystallization during solid state flow: effects of stress and temperature. Geophysical Research Letters 25, 3457–3460.
de Bresser, J.H.P., ter Heege, J.H., Spiers, C.J., 2001. Grain size reduction by dynamic recrystallization: can it result in major rheological weakening? International Journal of Earth Sciences (Geologische Runschau) 90, 28–45.
de Bresser, J.H.P., Evans, B., Renner, J., 2002. On estimating the strength of calcite rocks under natural conditions. In: de Meer, S., Drury, M.R., de Bresser, J.H.P., Pennock, G.M. (Eds.), Deformation Mechanisms, Rheology and Tectonics: Current Status and Future Perspectives. Geological Society Special Publications 200, pp. 309–329.
Derby, B., Ashby, M.F., 1987. On dynamic recrystallization. Scripta Metallurgica 21, 879–884.
Dresen, G., Evans, B., Olgaard, D.L., 1998. Effect of quartz inclusions on plastic flow in marble. Geophysical Research Letters 25, 1245–1248.
Drury, M.R., Urai, J.L., 1990. Deformation-related recrystallization processes. Tectonophysics 172, 235–253.
Evans, B., Renner, J., Hirth, G., 2001. A few remarks on the kinetics of static grain growth in rocks. International Journal of Earth Sciences (Geologische Rundschau) 90, 88–103.
Fueten, F., 1997. A computer-controlled rotating polarizer stage for the petrographic microscope. Computers & Geosciences 23, 203–308.
Fueten, F., Goodchild, J.S., 2001. Quartz c-axes orientation determination using the rotating polarizer microscope. Journal of Structural Geology 23, 895–902.
Gilman, J.J., 1960. Direct measurements of the surface energies of crystals. Journal of Applied Physics 31, 2208.
Goodchild, J.S., Fueten, F., 1998. Edge detection in petrographic images using the rotating polarizer stage. Computer & Geosciences 24, 745–751.
Handy, R.M., 1992. Correction and addition to "The Solid-State Flow of Polymineralic Rocks". Journal of Geophysical Research 97, 1897–1899.
Heilbronner, R., Bruhn, D., 1999. The influence of three-dimensional grain size distributions on the rheology of polyphase rocks. Journal of Structural Geology 20, 695–707.
Herwegh, M., 2000. A new technique to automatically quantify microstructures of fine grained carbonate mylonites: two step etching combined with SEM imaging and image analysis. Journal of Structural Geology 22, 391–400.
Herwegh, M., Jenni, A., 2001. Granular flow in polymineralic rocks bearing sheet silicates: new evidences from natural examples. Tectonophysics 332, 309–320.
Herwegh, M., Kunze, K., 2002. The influence of nano-scale second-phase particles on deformation of fine grained calcite mylonites. Journal of Structural Geology 24, 1463–1478.
Herwegh, M., Handy, M.R., Heilbronner, R., 1997. Temperature and strain rate dependent microfabric evolution in monomineralic mylonite: evidence from in situ deformation of a rock analogue. Tectonophysics 280, 83–106.
Hull, D., Bacon, D., 1984. Introduction to Dislocations. Pergamon Press, Oxford, 257pp.
Ji, S., Wang, Z., Wirth, R., 2001. Bulk flow strength of forsterite–enstatite composites as a function of forsterite content. Tectonophysics 341, 69–93.
Karato, S., Masuda, T., 1989. Anisotropic grain growth in quartz aggregates under stress and its implication for foliation development. Geology 17, 695–698.
Knipe, R.J., 1989. Deformation mechanisms—recognition from natural tectonites. Journal of Structural Geology 11, 127–146.
Krabbendam, M., Urai, J.L., van Vliet, L.J., 2003. Grain size stabilisation by dispersed graphite in a high-grade quartz mylonite: an example from Naxos (Greece). Journal of Structural Geology 25, 855–866.
Kretz, R., 1994. Metamorphic Crystallization. John Wiley, Chichester, 507pp.
Kruhl, J.H., 2001. Crystallographic control on the development of foam textures in quartz, plagiocalse and analogue material. International Journal of Earth Sciences (Geol Runsch) 90, 104–117.
Kruhl, J.H., Peternell, M., 2002. The equilibration of high-angle grain boundaries in dynamically recrystallized quartz; the effect of crystallography and temperature. Journal of Structural Geology 24, 1125–1137.
Kruse, R., Stünitz, H., 1999. Deformation mechanisms and phase distribution in mafic high-temperature mylonites from the Jotun Nappe, southern Norway. Tectonophysics 303, 223–249.
Lister, G.S., Snoke, A.W., 1984. S–C mylonites. Journal of Structural Geology 6, 617–638.
Mauler, A., Godard, G., Kunze, K., 2001. Crystallographic fabrics of omphacite, rutile and quartz in Vende'e eclogites (Armorican Massif, France). Consequences for deformation mechanisms and regimes. Tectonophysics 342, 81–112.
Means, W.D., 1981. The concept of steady-state foliation. Tectonophysics 78, 179–199.
Mercier, J.C., Anderson, D.A., Carter, N.L., 1977. Recrystallization and stress in the lithosphere. Pure and Applied Geophysics 115, 199–226.
Nes, E., Ryum, N., Hunderi, O., 1985. On the Zener drag. Acta Metallurgica 33, 11–22.
Nicolas, J., Poirier, J.P., 1976. Crystalline Plasticity and Solid State Flow in Metamorphic Rocks. Wiley-Interscience, 444pp.
Olgaard, D.L., 1990. The role of second-phase in localizing deformation. In: Knipe, R.J., Rutter, E.H. (Eds.), Deformation Mechanisms, Rheology and Tectonics. Geological Society Special Puplication 54, pp. 175–181.
Paterson, M.S., 1973. Nonhydrostatic thermodynamics and its geological application. Reviews in Geophysics 11, 355–389.
Paterson, M.S., 1995. A theory of granular flow accommodated by material transfer via intergranular fluid. Tectonophysics 245, 135–151.
Pauli, C., Schmid, S.M., Panozzo-Heilbronner, R., 1996. Fabric domains in quartz mylonites: localized three-dimensional analysis of microstructure and texture. Journal of Structural Geology 18, 1183–1203.
Pfiffner, A.O., 1982. Deformation mechanisms and flow regimes in limestone from the Helvetic zone of the Swiss Alps. Journal of Structural Geology 4, 429–442.
Pieri, M., Burlini, L., Kunze, K., Stretton, I., Olgaard, D.L., 2001. Rheological and microstructural evolution of Carrara marble with high shear strain: results from high temperature torsion experiments. Journal of Structural Geology 23, 1393–1413.
Poirier, J.P., 1985. Creep of Crystals. Cambridge University Press, 260pp.
Rutter, E.H., 1995. Experimental study of the influence of stress, temperature, and strain on the dynamic recrystallization of Carrara marble. Journal of Geophysical Research 100, 24651–24663.
Ryum, N., Hunderi, O., Nes, E., 1983. On grain boundary drag from second-phase particles. Scripta Metallurgica 17, 1281–1283.
Schmid, S.M., Handy, M.R., 1991. Towards a genetic classification of fault rocks: geological usage and tectonophysical implications. In: Müller, D.W., McKenzie, J.A., Weissert, H. (Eds.), Contoversies in Modern Geology, Academic Press, London, pp. 95–110.

Schmid, S.M., Paterson, M.S., Boland, J.N., 1977. Superplastic flow in fine-grained limestone. Tectonophysics 43, 257–291.

Schmid, S.M., Paterson, M.S., Boland, J.N., 1980. High temperature flow and dynamic recrystallization in Carrara marble. Tectonophysics 65, 245–280.

Schoeck, G., 1995. The core energy of dislocations. Acta Metalurgica Materialia 43, 3679–3684.

Shimizu, I., 1998. Stress and temperature dependence of recrystallized grain size: a subgrain misorientation model. Geophysical Research Letters 25, 4237–4240.

Smith, C.S., 1948. Grains, phases, and interphases: an interpretation of microstructure. Transactions American Institute of Mining and Metallurgical Engineering 175, 15–51.

Spry, A., 1969. Metamorphic Textures. Pergamon Press, 350pp.

Stünitz, H., 1998. Syndeformational recrystallization: dynamic or compositionally induced? Contributions to Mineralogy and Petrology 131, 219–236.

Stüwe, H.P., 1978. Driving and dragging forces in recrystallization. In: Haessner, F., (Ed.), Recrystallization of Metallic Materials, Riederer Verlag, Stuttgart, pp. 11–21.

ter Heege, J.H., 2002. Relationship between dynamic recrystallization, grain size distribution and rheology. Geologica Ultraiectina 218, 141.

Tullis, T.E., Horowitz, F.G., Tullis, J., 1991. Flow laws of polyphase aggregates from end-member flow laws. Journal of Geophysical Research 96, 8081–8096.

Tungatt, P.D., Humphreys, F.J., 1981. An in situ optical investigation of the deformation behavior of sodium nitrate—an analogue for calcite. Tectonophysics 78, 661–676.

Twiss, R.J., 1977. Theory and applicability of a recrystallized grain size palaepiezometer. Pure and Applied Geophysics 115, 227–244.

Underwood, E.E., 1970. Quantitative Stereology. Addison Wesley, Reading, Massachusetts, 274pp.

Voll, G., 1961. Zur Frage des Stofftransports auf den Korngrenzen metamorpher Gesteine. Geol. Rdsch 51, 395–405.

Walker, A.N., Rutter, E.H., Brodie, K.H., 1990. Experimental study of grain-size sensitive flow of synthetic, hot pressed calcite rocks, In: Knipe, R.J., Rutter, E.H. (Eds.), Deformation Mechanisms, Rheology and Tectonics. Geological Society Special Puplication 54, pp. 259–284.

Wertmann, J., Wertmann, J.R., 1992. Elementary Dislocation Theory. Oxford University Press, Oxford, 213pp.

White, S.H., 1977. Geological significance of recovery and recrystallization processes in quartz. Tectonophysics 39, 143–170.